Debonding behavior of a single leg bending specimen

This example examines the debonding behavior of a single leg bending specimen.

The following Abaqus features are demonstrated:

- predicting debond growth in a single leg bending (SLB) specimen using crack propagation analysis with the VCCT fracture criterion in Abaqus/Standard;
- predicting debond growth using the VCCT fracture criterion and surface-based cohesive behavior in Abaqus/Explicit; and
- predicting progressive delamination growth at the interface in this specimen subjected to subcritical cyclic loading using the traditional fatigue crack growth criterion and the PRX-Fatigue crack growth criterion, both based on the Paris law.

This page discusses:

- Application description
- Abaqus modeling approaches and simulation techniques
- Case 1 Two-dimensional single leg bending model
- Case 2 Three-dimensional single leg bending model
- Case 3 Fatigue prediction using the same model as in Case 1
- Case 4 Fatigue prediction using the same model as in Case 2
- Case 5 Using VCCT in Abaqus/Explicit to model crack initiation
- Input files
- References
- Figures

Products: Abaqus/Standard Abaqus/Explicit

Application description

The example examines the debonding behavior of a single leg bending specimen and compares the simulation results with the results of the analysis performed using the VCCT-based fracture interface elements discussed in Mabson (2003). Damping is also used in a two-dimensional model to demonstrate how it can stabilize the crack growth.

The same model is analyzed using the fatigue crack growth criterion to assess the fatigue life when the model is subjected to subcritical cyclic loading. The onset and delamination growth are characterized using the Paris law, which relates the relative fracture energy release rate to the crack growth rate. The fracture energy release rate at the crack tip is calculated based on the VCCT technique. The results from Abaqus are compared with those predicted by the theory in Davidson (1995).

Geometry

The geometries of the two-dimensional and three-dimensional single leg bending specimens with their corresponding initial crack locations are shown in Figure 1 and Figure 2, respectively.

Boundary conditions and loading

A displacement is applied on the top beam at the location shown in Figure 1 for the two-dimensional model and in Figure 2 for the three-dimensional model. The displacement results in a mixture of opening (mode I) and shearing (mode II) modes. The maximum displacements are set equal to 0.32 in (8.13 mm) in the two-dimensional model and 0.15 in (3.81 mm) in the three-dimensional model for the monotonic loading cases. In the fatigue crack growth analyses, cyclic displacement loadings with peak values of 0.12 in (3.05 mm) in the two-dimensional model and 0.035 in (0.89 mm) in the three-dimensional model are specified.

Abaqus modeling approaches and simulation techniques

This example includes one two-dimensional model and one three-dimensional model.

Summary of analysis cases

Case 1	Two-dimensional single leg bending model.
Case 2	Three-dimensional single leg bending model.
Case 3	Fatigue prediction with the direct cyclic approach, the linear elastic fatigue crack growth approach, and the PRX-Fatigue approach using the same model as in Case 1.
Case 4	Fatigue prediction with the direct cyclic approach, the linear elastic fatigue crack growth approach, and the PRX-Fatigue approach using the same model as in Case 2.
Case 5	Abaqus/Explicit with VCCT using the same model as in Case 2.

Analysis types

Static analyses are performed for Cases 1–4. Dynamic analysis is used for Case 5.

Case 1 Two-dimensional single leg bending model

This case compares the AbaqusVCCT results for the two-dimensional model with the results of Mabson (2003). The damping effects are also examined.

Mesh design

The model uses a finite element mesh of 4-node bilinear plane strain quadrilateral, incompatible mode elements (CPE4I) for both the long and short beams.

Results and discussion

Figure 3 shows the deformed configuration of the two-dimensional model. Figure 4 shows a contour plot of bond status variable BDSTAT that illustrates the debonding growth in a two-dimensional model. The region of debonding is shown on the right side of the model. Figure 5 compares the results from the two-dimensional analysis with the results of the analysis performed using the VCCT-based fracture interface elements discussed in Mabson (2003).

The damping effect to a two-dimensional simulation is also examined in this case by adding damping at the debond interface (see Automatic Stabilization of Rigid Body Motions in Contact Problems). The damping stabilizes the crack growth and allows the solution to converge. It is important to assess how much energy has been used for numerical damping by comparing the stabilization energy to the strain energy of the model. Figure 6 shows the comparison between static stabilization energy (ALLSD) and the strain energy of the model (ALLSE). The comparison indicates that the maximum static stabilization energy is less than 3% of the maximum strain energy of the model during the analysis. This value is reasonable and indicates that the solution has not been affected by the addition of artificial numerical damping.

Case 2 Three-dimensional single leg bending model

This case compares the AbaqusVCCT results for the three-dimensional model with a theoretical prediction.

Mesh design

The model uses fully integrated first-order shell elements (S4) for both the long and short beams.

Results and discussion

Figure 7 shows a contour plot of bond status variable BDSTAT for the three-dimensional model. Figure 8 shows a comparison between the results from the three-dimensional analysis and the results presented in Mabson (2003).

Case 3 Fatigue prediction using the same model as in Case 1

This case verifies that delamination growth in a two-dimensional single leg bending model subjected to subcritical cyclic loading can be predicted using the fatigue crack growth criterion. The direct cyclic approach, the linear elastic fatigue crack growth approach, and the PRX-Fatigue approach are used for this case study

Mesh design

The mesh design is the same as in Case 1.

Results and discussion

The simulation results for the direct cyclic approach are compared with the theoretical results in Figure 9, which shows the crack length versus the number of cycles. Reasonably good agreement is obtained between the simulation and the theoretical results. The corresponding simulation results using the linear elastic fatigue crack growth and the PRX-Fatigue approaches are close to the results obtained using the direct cyclic approach and are not shown here.

Case 4 Fatigue prediction using the same model as in Case 2

This case verifies that delamination growth in a three-dimensional single leg bending model subjected to subcritical cyclic loading can be predicted using the fatigue crack growth criterion with the debonding force removed immediately or ramped down gradually. The direct cyclic approach, the linear elastic fatigue crack growth approach, and the PRX-Fatigue approach are used in this case study.

Mesh design

The mesh design is the same as in Case 2.

Results and discussion

The simulation results using the direct cyclic approach are compared with the theoretical results in Figure 10, which shows the crack length versus the number of cycles. Reasonably good agreement is obtained between the simulation and the theoretical results. The corresponding simulation results using the linear elastic fatigue crack growth and the PRX-Fatigue approaches are close to the results obtained using the direct cyclic approach and are not shown here.

Case 5 Using VCCT in Abaqus/Explicit to model crack initiation

This case verifies that delamination growth can be predicted using Abaqus/Explicit. The simulation results are compared with results obtained from Abaqus/Standard. To reduce inertia effects and allow a better comparison between Abaqus/Standard and Abaqus/Explicit results, the material density was lowered and the loading was ramped on with a smooth step definition.

Mesh design

The mesh design is the same as in Case 2.

Results and discussion

The results obtained using Abaqus/Explicit with VCCT show reasonably good agreement with those obtained from Abaqus/Standard, as depicted in Figure 11 and Figure 12. Due to the thin layer of elements and the specified boundary conditions in the model, inertia effects are clearly observed in the measured reaction forces. However, the peak forces at debond onset, debond time, and other VCCT output quantities are consistent between the two analyses. The reaction forces obtained in Abaqus/Explicit were filtered with a Butterworth filter with a cutoff frequency of 500 Hz to reduce high-frequency oscillations from the response curve.

Input files

slb_vcct_2d_1.inp

Two-dimensional model of the SLB specimen.

slb_vcct_3d_1.inp

Three-dimensional model of the SLB specimen.

slb_vcct_fatigue_2d.inp

Same as `slb_vcct_2d_1.inp` but subjected to cyclic displacement loading using the direct cyclic approach.

slb_vcct_fatigue_2d_2_simp.inp

Same as `slb_vcct_2d_1.inp` but subjected to cyclic displacement loading using the simplified fatigue crack growth approach.

slb_vcct_fatigue_2d_2_simp_prx.inp

Same as `slb_vcct_2d_1.inp` but subjected to cyclic displacement loading using the simplified PRX-Fatigue approach.

slb_vcct_fatigue_2d_3_simp_tabular.inp

Same as `slb_vcct_2d_1.inp` but subjected to cyclic displacement loading using the simplified fatigue crack growth approach with the tabular form.

slb_vcct_fatigue_2d_3_tabular_prx.inp

Same as `slb_vcct_2d_1.inp` but subjected to cyclic displacement loading using the general PRX-Fatigue approach with the tabular form.

slb_vcct_fatigue_2d_3_simp_user.inp

Same as `slb_vcct_2d_1.inp` but subjected to cyclic displacement loading using the simplified fatigue crack growth approach with the user-defined subroutine.

slb_vcct_fatigue_3d_2_simp_prx.inp

Same as `slb_vcct_3d_1.inp` but subjected to cyclic displacement loading using the simplified PRX-Fatigue approach.

slb_vcct_fatigue_2d_3_tabular.inp

Same as `slb_vcct_2d_1.inp` but subjected to cyclic displacement loading using the general fatigue crack growth approach with the tabular form.

slb_vcct_fatigue_3d_3_tabular_prx.inp

Same as `slb_vcct_3d_1.inp` but subjected to cyclic displacement loading using the general PRX-Fatigue approach with the tabular form.

slb_vcct_fatigue_2d_3_user.inp

Same as `slb_vcct_2d_1.inp` but subjected to cyclic displacement loading using the general fatigue crack growth approach with the user-defined subroutine.

slb_vcct_fatigue_3d.inp

Same as `slb_vcct_3d_1.inp` but subjected to cyclic displacement loading using the direct cyclic approach.

slb_vcct_fatigue_3d_2_simp.inp

Same as `slb_vcct_3d_1.inp` but subjected to cyclic displacement loading using the simplified fatigue crack growth approach.

slb_vcct_fatigue_3d_3_simp_tabular.inp

Same as `slb_vcct_3d_1.inp` but subjected to cyclic displacement loading using the simplified fatigue crack growth approach with the tabular form.

slb_vcct_fatigue_3d_3_simp_user.inp

Same as `slb_vcct_3d_1.inp` but subjected to cyclic displacement loading using the simplified fatigue crack growth approach with the user-defined subroutine.

slb_vcct_fatigue_3d_3_tabular.inp

Same as `slb_vcct_3d_1.inp` but subjected to cyclic displacement loading using the general fatigue crack growth approach with the tabular form.

slb_vcct_fatigue_3d_3_user.inp

Same as `slb_vcct_3d_1.inp` but subjected to cyclic displacement loading using the general fatigue crack growth approach with the user-defined subroutine.

slb_vcct_fatigue_3d_3_simp_tabular_ramp.inp

Same as `slb_vcct_fatigue_3d_3_simp_tabular.inp` but with the debonding force ramped down gradually.

slb_vcct_fatigue_3d_3_simp_user_ramp.inp

Same as `slb_vcct_fatigue_3d_3_simp_user.inp` but with the debonding force ramped down gradually.

slb_vcct_fatigue_3d_3_tabular_ramp.inp

Same as `slb_vcct_fatigue_3d_3_tabular.inp` but with the debonding force ramped down gradually.

slb_vcct_fatigue_3d_3_user_ramp.inp

Same as `slb_vcct_fatigue_3d_3_user.inp` but with the debonding force ramped down gradually.

slb_vcct_xpl_3d.inp

Three-dimensional model of the SLB specimen using Abaqus/Explicit with VCCT.

References

Mabson, G, "Fracture Interface Elements," 46th PMC General Session of Mil-17 (Composites Materials Handbook) Organization, Charleston, SC, 2003.

Davidson, B. D., R. Kruger, and M. Konig, "Three-Dimensional Analysis of Center-Delaminated Unidirectional and Multidirectional Single-Leg Bending Specimens," Composites Science and Technology, vol. 54, pp. 385–394, 1995.

Figures

Figure 1. The two-dimensional single leg bending (SLB) specimen.

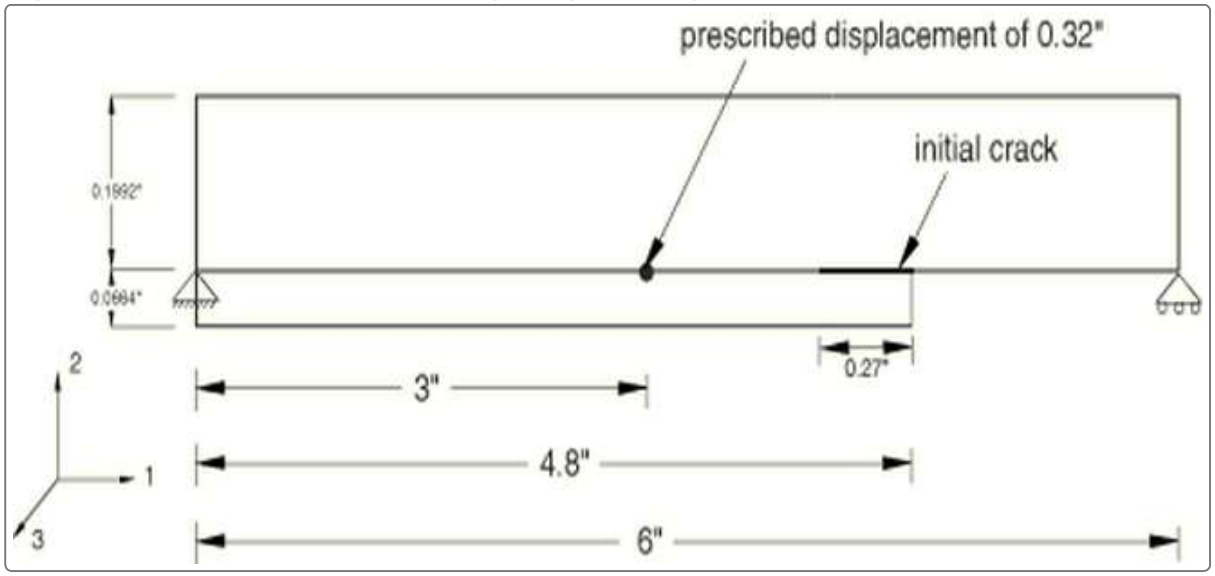

Figure 2. The three-dimensional single leg bending (SLB) specimen.

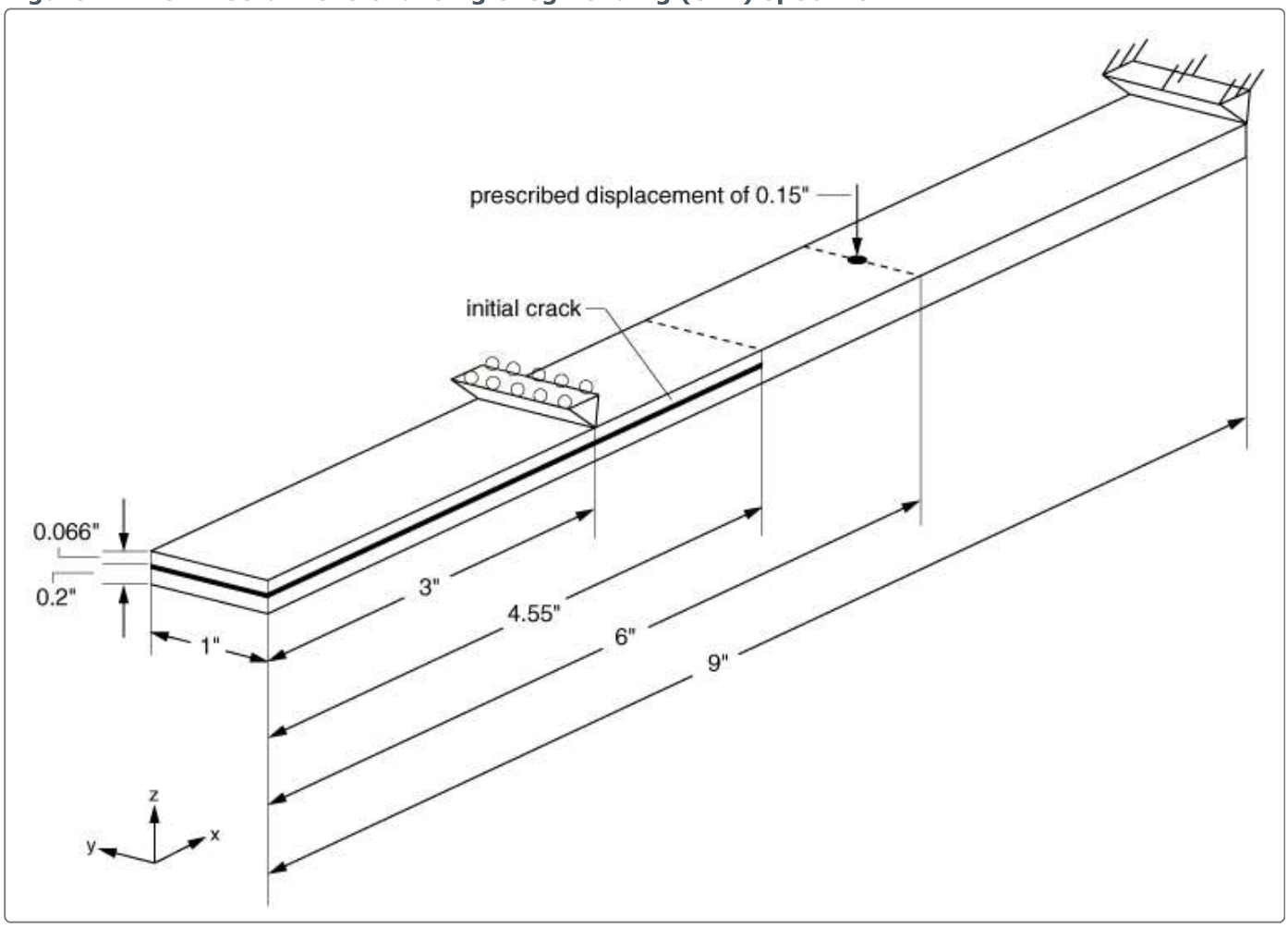

Figure 3. The deformed shape of the two-dimensional model showing boundary conditions and prescribed displacements.

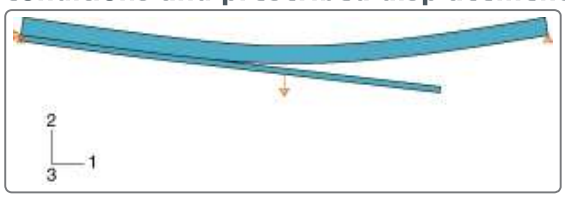

Figure 4. The prediction of debonding growth for the two-dimensional SLB model.

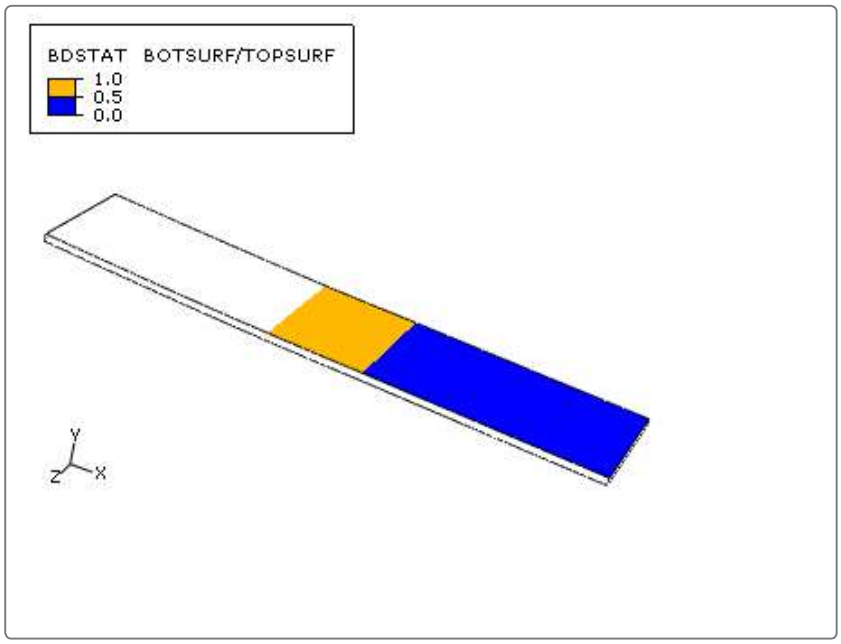

Figure 5. Response prediction for the two-dimensional SLB model.

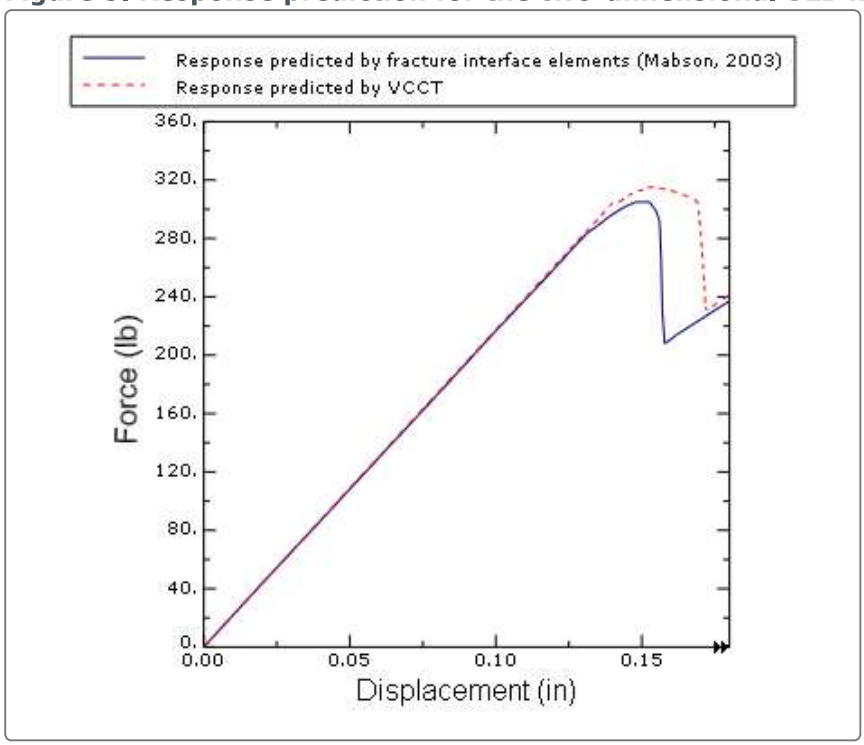

Figure 6. A comparison between ALLSD and ALLSE for the two-dimensional model.

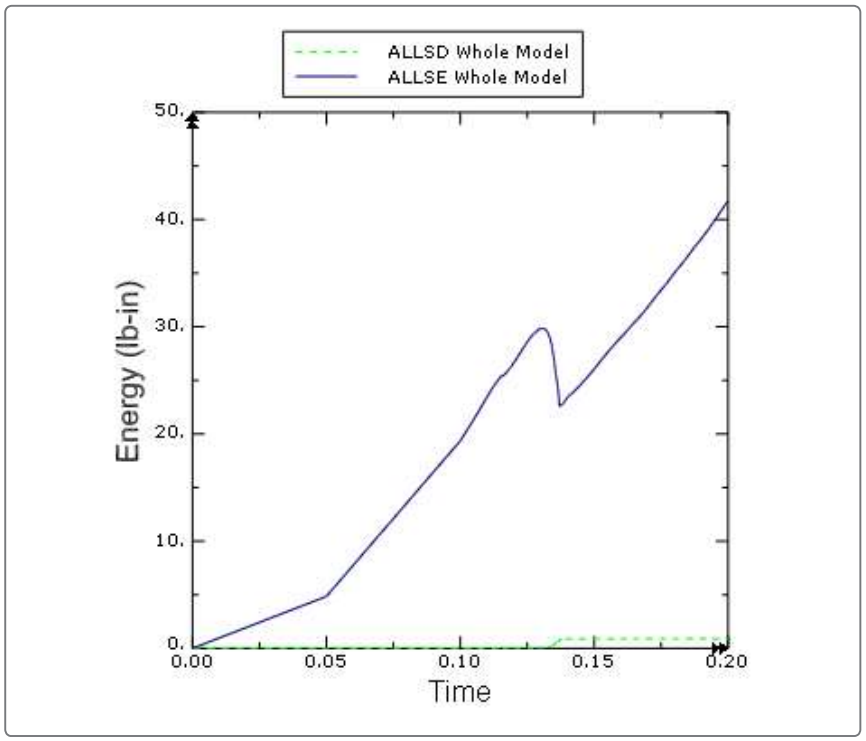

Figure 7. The prediction of debonding growth for the three-dimensional SLB model.

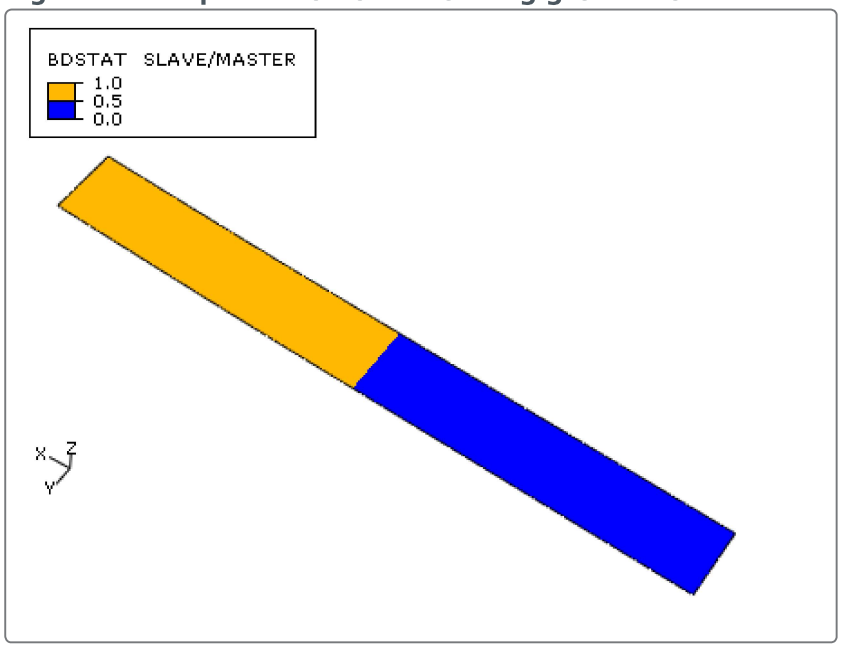

Figure 8. Response prediction for the three-dimensional SLB model.

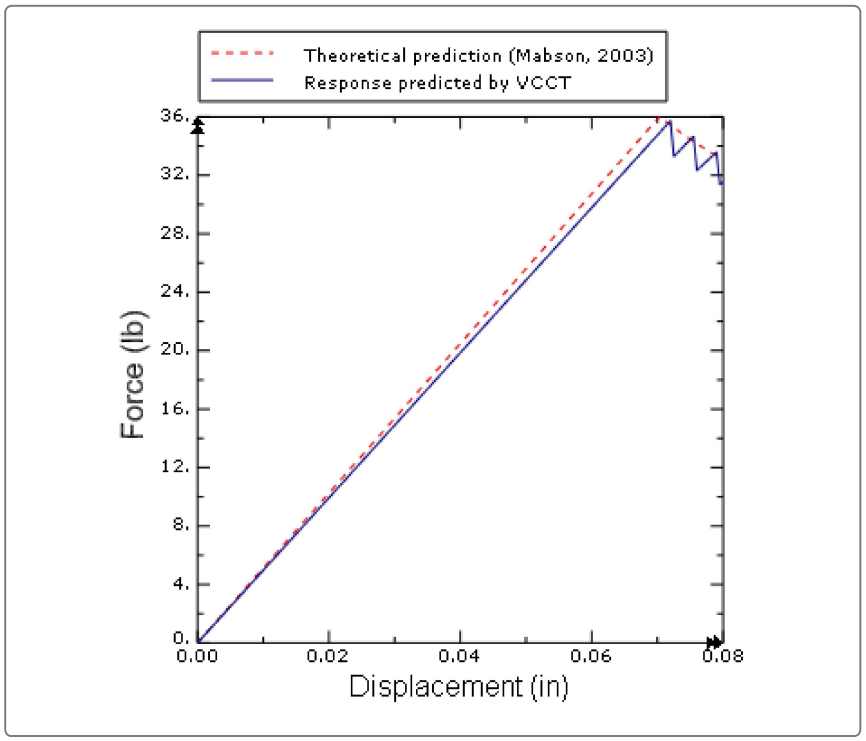

Figure 9. Crack length versus cycle number for the two-dimensional SLB model.

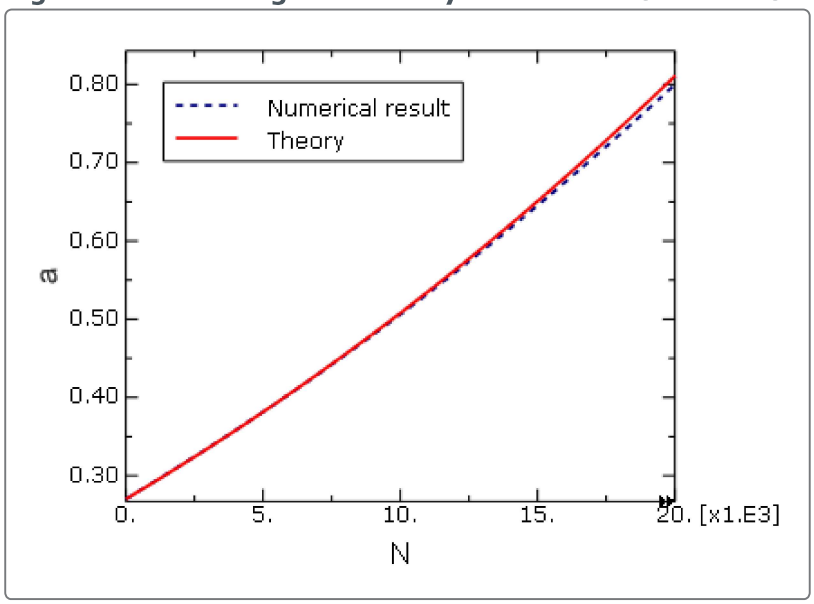

Figure 10. Crack length versus cycle number for the three-dimensional SLB model.

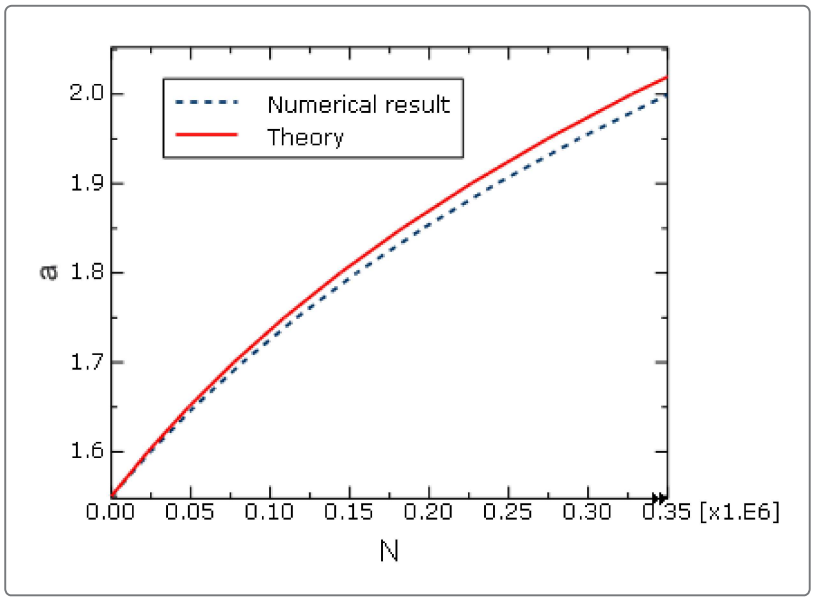

Figure 11. Debond state comparison between Abaqus/Explicit (top) and Abaqus/Standard (bottom).

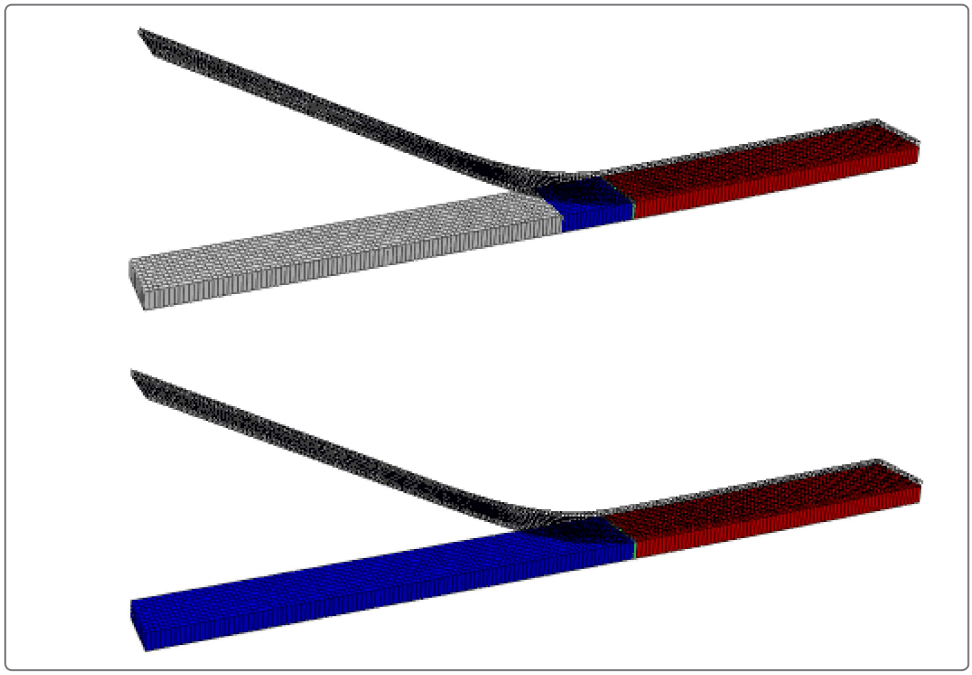

Figure 12. Comparison of the results between Abaqus/Explicit and Abaqus/Standard.

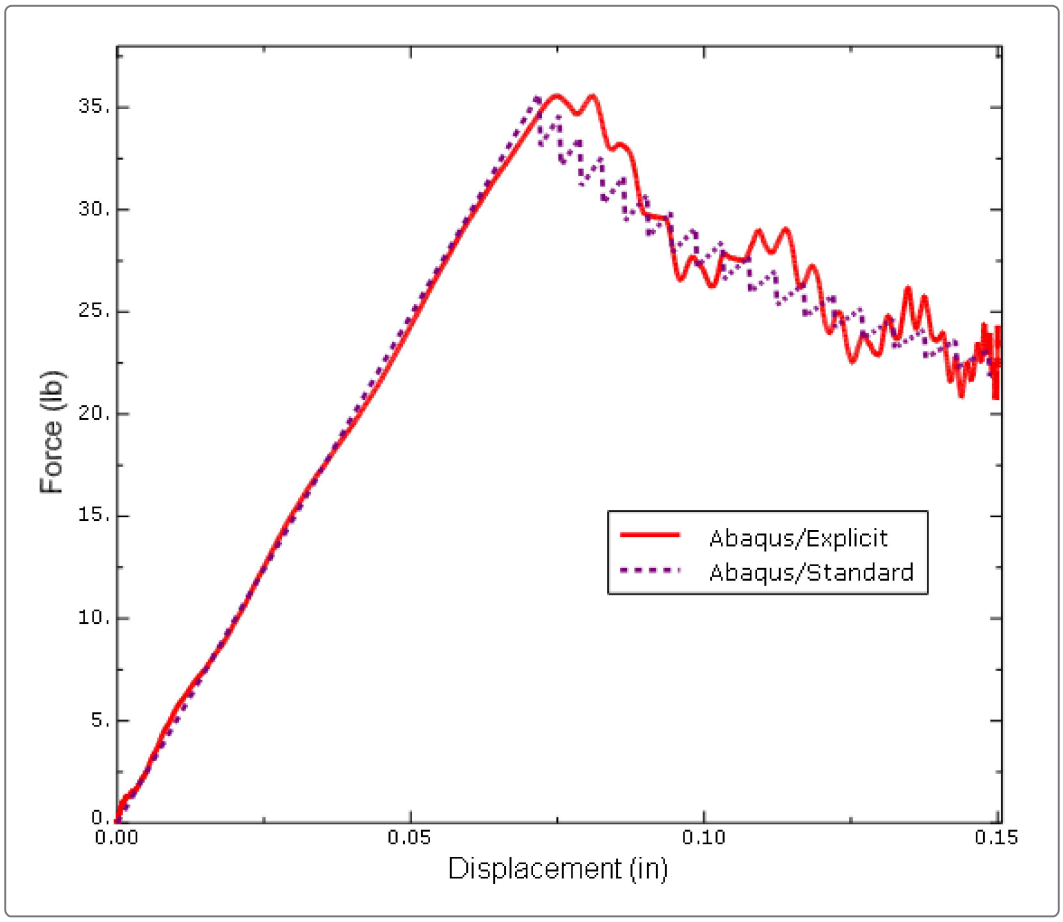
Force (lb)
35.
30.
25.
20.
15.
10.
5.
0.
0.00
0.05
0.10
0.15
Displacement (in)
Abaqus/Explicit
Abaqus/Standard